Title

Vortex circulation patterns in planar microdisk arrays (vol 110, 262406, 2017)

Journal

APPLIED PHYSICS LETTERS, 111(5)

ISSN

0003-6951

Authors

Velten, Sven
Streubel, Robert
Farhan, Alan
et al.

Publication Date

2017

Peer reviewed

Vortex circulation patterns in planar microdisk arrays

Sven Velten,[1,2,a)] Robert Streubel,[1,b)] Alan Farhan,[3] Noah Kent,[1,4] Mi-Young Im,[1,5] Andreas Scholl,[3] Scott Dhuey,[6] Ulrich Merkt,[2] Carolin Behncke,[2] Guido Meier,[7] and Peter Fischer[1,4]

[1)] *Materials Sciences Division, Lawrence Berkeley National Laboratory, 1 Cyclotron Road, Berkeley, California 94720, USA.*

[2)] *Institut für Nanostruktur- und Festkörperphysik, Universität Hamburg, Jungiusstrasse 11, 20355 Hamburg, Germany.*

[3)] *Advanced Light Source, Lawrence Berkeley National Laboratory, 1 Cyclotron Road, Berkeley, California 94720, USA.*

[4)] *Physics Department, University of California, 1156 High Street, Santa Cruz, California 95064, USA.*

[5)] *Daegu Gyeongbuk Institute of Science and Technology, Daegu 711-873, Korea.*

[6)] *Molecular Foundry, Lawrence Berkeley National Laboratory, 1 Cyclotron Road, Berkeley, California 94720, USA.*

[7)] *Max-Planck Institute for the Structure and Dynamics of Matter, Luruper Chaussee 149, 22761 Hamburg, Germany.*

(Dated: April 17, 2017)

We report a magnetic X-ray microscopy study of the pattern formation of the circulation in arrays of magnetic vortices ordered in a hexagonal and a honeycomb lattice, respectively. In the honeycomb lattice we observe at remanence an ordered phase of alternating circulations, whereas in the hexagonal lattice small regions of alternating lines form. A variation of the edge-to-edge distance shows that the size of those regions scales with the magnetostatic interaction. Micromagnetic simulations reveal that the patterns result from the formation of flux closure states during the nucleation process.

The coupling of magnetic nanostructures in lateral arrangements leads to a collective behavior of the spin textures, which results for example in exotic phase transitions, such as the spin ice phase[1], or specific spectra for spin excitations in so-called magnonic crystals[2,3]. Recently chiral spin textures have stepped into the spotlight due to their possible impact on spintronic devices[4–7]. Those spin textures can be formed as a result of confinement in magnetic structures. Examples are magnetic vortices, that are formed in circular microdisks. Such a vortex has a circulating in-plane texture (circulation), that can rotate clockwise or counter-clockwise, and a vortex core at its center (polarization), that can point up or down. The orientation of both circulation (clockwise/counter-clockwise) and polarization (up/down) are a-priori randomly generated in isolated disks. However, when arranged in arrays, magnetic vortices are coupled due to magneto-static interactions arising if an external magnetic field is applied. This leads to a collective ordering of the polarization states, if the magnetic field is oscillating with specific frequencies[8,9]. Moreover, the vortex core excitation spectrum reveals band-structure like behavior[10,11]. For circulation states, patterns are reported after applying a strong magnetic field pulse to disk pairs[12] or to arrays of curved thin film structures[13,14]. The formation of those patterns is affected by the coupling strength and thermal excitations. However, a profound study of the vortex circulation pattern as a function of the interplay between magnetostatics and thermal fluctuations is still lacking.

Here, we report an investigation of arrays of planar disks ordered in hexagonal and honeycomb lattices. We study the formation of the patterns in the circulation of the magnetic vortices by high resolution magnetic soft X-ray microscopy. By systematically varying the lattice constant and thus the strengths of the magneto-static interaction between neighboring disks, we observe a clear impact on the pattern formation and pattern size. Our findings prove that the pattern formation takes place on a completely different energy scale than the alternation of vortex annihilation and nucleation fields[15].

The microdisk arrays were lithographically patterned utilizing electron beam lithography with low exposure dose and ultrasonic agitation at room temperature development to promote the removal of degraded molecules[16] and to provide the required spatial resolution for fabricating well defined microstructures. Disks with a diameter of 1 µm and an edge-to-edge spacing d_e ranging from 200 nm down to 70 nm were arranged into areas of 25 µm × 25 µm with hexagonal or honeycomb symmetry. Electron beam evaporation of permalloy (Py, $Ni_{80}Fe_{20}$) followed by lift off led to 40 nm thin soft-magnetic disks of the desired geometry. Images of the structures with their symmetry directions [10] and [01] are shown in figures 1(a,b). In those Py disks, the magnetic vortex ground state is favored that arranges in certain patterns throughout the disk array, as illustrated in figures 1(c,d).

The interaction responsible for the pattern formation is of pure magneto static nature[17]. Whereas the remanent vortex state is virtually stray field free, small lateral displacements induced by an external magnetic field of the vortex core cause surface charges at the

[a)] E-mail:svelten@physnet.uni-hamburg.de

[b)] E-mail:streubel@lbl.gov

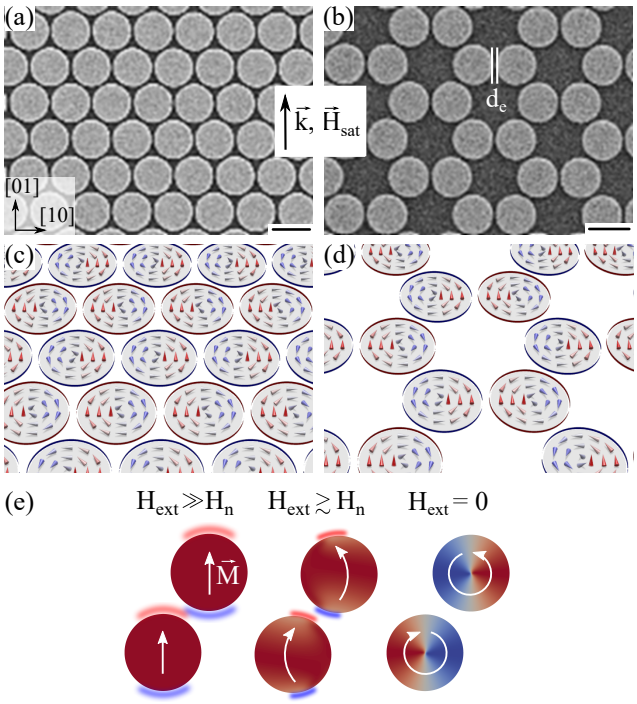

Figure 1. Scanning electron micrographs the vortex lattices with edge-to-edge distance $d_e = 70\,\text{nm}$ for the (a) hexagonal lattice and (b) honeycomb lattice. The illustrated symmetry directions [10] and [01] are valid for both lattices. The inset in the middle illustrates the wavevector component $\vec{k}$ of the incident X-rays, which lies in the sample plane, and the direction of the external magnetic field $\vec{H}_{sat}$. Scale bars indicate 1 µm. Schematics of the magnetic ground state at remanence in the (c) hexagonal and (d) honeycomb disk array. In both cases the circulation states (either clockwise or counter-clockwise) of the vortices form patterns. (e) Micromagnetic simulation of a diagonal vortex pair with a decreasing external field H_{ext} from a magnitude much bigger than the nucleation field H_n (left picture) to remanence (right). Also shown is the nucleation state (middle). The local magnetization is illustrated by a white arrow and the colorized disk with a red (parallel to $\vec{k}$, as indicated in the mid-inset above) to blue (antiparallel) contrast. Positive and negative magnetic surface charges are highlighted by red and blue shadows, respectively.

disk edges ($\sigma(\vec{r}) = \vec{M}(\vec{r}) \cdot \vec{n}(\vec{r})$, with local magnetization $\vec{M}(\vec{r})$ and surface normal $\vec{n}(\vec{r})$) that are largest during the vortex nucleation process when applying in-plane magnetic fields larger than the annihilation/nucleation fields. In individual and perfectly isolated magnetic vortex structures the selection of polarity and circulation is completely random. This degeneracy is lifted in arrangements of magnetostatically interacting vortices, e.g. pairs. There, the circulation is predetermined by the orientation of the in-plane magnetic field relative to the pair[12]. An exemplary simulation of the nucleation process of diagonal aligned vortices is shown in figure 1(e). The micromagnetic simulations are performed by using Nmag v.0.2[18], the Hlib library[19,20] and typical material parameter for Py[21]: Saturation magnetization $M_s = 860\,\text{kA/m}$ and exchange stiffness $A = 1.3 \times 10^{-11}\,\text{J/m}$. The interaction between surface charges in the saturated state (left picture) results in a flux closure state, when the external field is lowered to the regime of the nucleation field (middle). At remanence, the circulations are alternatingly ordered (right). A change of the orientation of the external field would decrease the interaction strength and thus would make the formation of the flux closure state less favorable.

This scheme provides means to tailor the vortex circulation pattern throughout an entire array with certain structural symmetry. Figure 2 depicts the vortex circulation patterns at remanence after saturating along the [01] (figures 2(a,c)) and [10] (figures 2(b,d)) direction. The results are obtained by utilizing magnetic transmission X-ray microscopy (MTXM) and X-ray photoemission electron microscopy (X-PEEM), both located at the Advanced Light Source (ALS) in Berkeley CA. Tuning the circularly polarized X-rays to the Fe L_3-edge (706.8 eV) a magnetic contrast is measured due to the X-ray magnetic circular dichroism (XMCD). The effect provides an absorption dependency of the relative orientation of the incident photon helicity and the local magnetization. The wavevector component $\vec{k}$ of the photons in the sample plane is depicted in figure 1. Dark areas in the XMCD pictures refers to a magnetization parallel to $\vec{k}$, whereas an antiparallel alignment is obtained in bright areas.

The honeycomb array previously saturated along [01] (figure 2(a)) shows an extended alternating circulation pattern as expected beforehand (figure1(d)) due to flux closure states throughout the lattice during the nucleation (middle picture in figure 1(e)). A saturation along [10], however, results in a disappearance of the pattern (figure 2(b)). The lack of diagonal neighbors along the flux closure chains destabilizes the ordering. Additionally, competing interactions with its two diagonal neighbors lead to the phenomenon of a frustrated circulation state of a disk. This was firstly reported in hemispherical cap structures[13]. As a consequence, the result is a disordered circulation pattern.

The hexagonal array shows a completely different behavior. For both saturation directions, the circulation states in the hexagonal lattice form an alternating line pattern (figures 2(c,d)). They are a consequence of the combination of stray field minimization and circulation frustration. The flux closure states during the nucleation are built throughout the lattice, which generates the alternating line pattern. This competes with the tendency to disorder due to the existence of competing interactions of the diagonal neighbors. Hence, the ordering is only extended over small regions, nucleating around lattice defects and imperfect disks. The region size is a result of the interplay of thermal fluctuations and magnetostatic interaction strength and should therefore vary with varying temperature.

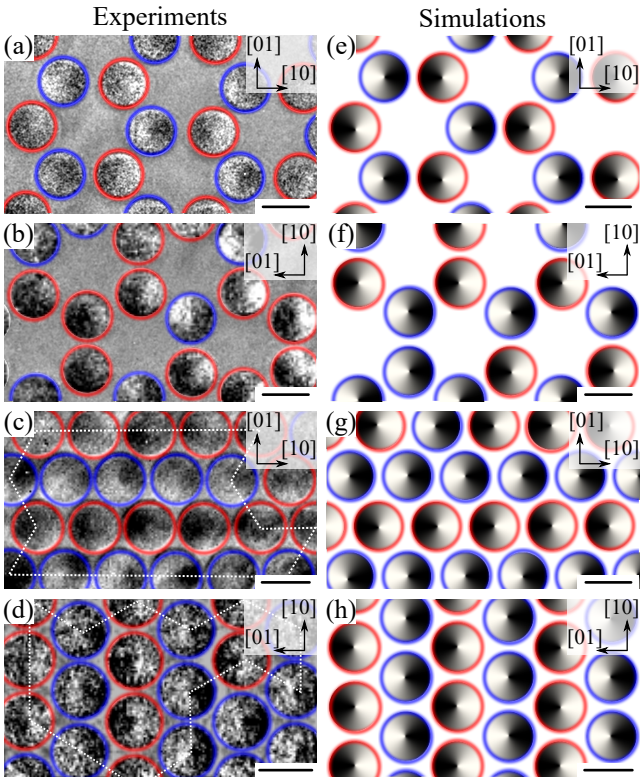

Figure 2. MTXM results for a (a,b) honeycomb and (c,d) hexagonal vortex lattice. The disks are previously saturated along the direction of $\vec{H}_{sat}$ ([01] in (a,c) and [10] in (b,d)). The disks are highlighted in red or blue to indicate a clockwise or counter-clockwise vortex circulation. (e-h) Corresponding micromagnetic simulation results. Scale bars indicate 1 µm.

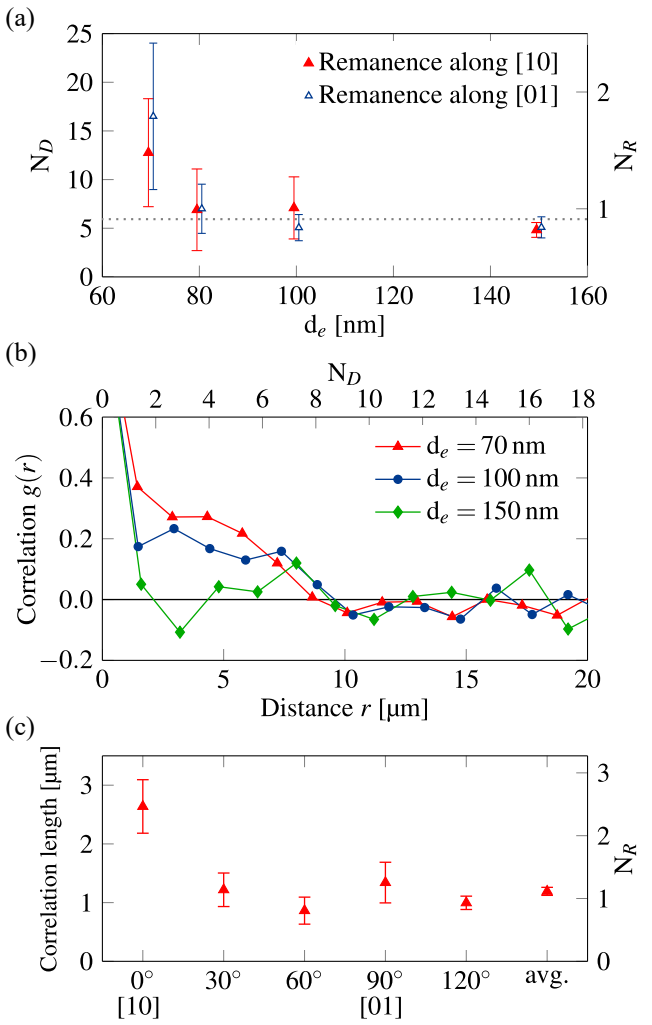

Figure 3. (a) Average number of disks N_D in the alternating line regions in the hexagonal lattices as a function of the edge-to-edge distance d_e obtained by MTXM measurements. The gray dotted line illustrates a random distribution of circulation states (disks are not interacting). (b) Spatial correlation along [10], when the lattice was saturated along [01], as a function of the distance and the number of disks N_D along the axis for different d_e. Calculated from X-PEEM measurements. (c) Derived correlation lengths along different major axes (0° = [10] and 90° = [01]), minor axes (30°, 60° and 120°) and the spatial average for the lattice with $d_e = 70$ nm, which was saturated along [01]. The spatial average corresponds to a measurement of the average radius of the circulation patterns, expressed in number of disks N_R. For comparison, this quantity is added as an axis in (a).

Figures 2(e-h) show the corresponding states obtained from micromagnetic simulations that are in very good agreement with the experimental results. Since lattice defects are lacking in the simulation, the patterns are expected to be suppressed in the hexagonal lattice, as they have no nucleation center to form around. Despite that, the alternating patterns are still formed in our simulations (figures 2(g,h)). The reasons are boundary effects in the simulated 6 disk times 6 disk array. Vortices at the lattice boundaries have a higher nucleation field because of weaker magnetostatic interaction[15]. A subsequent simulation with periodic boundary conditions resulted in random circulation states.

It is interesting to note that the lack of a proper mechanism to mimic temperature and thermal fluctuations in micromagnetic simulations does usually not influence the magnetic domains in transition metals due to significantly larger Curie temperatures. However, this statement is invalid for spatially separated magnetic films interacting via stray fields, resulting in our case in significantly larger vortex circulation patterns than experimentally observed at room temperature.

The pattern size is a parameter to measure the influence of thermal fluctuations and magnetostatic coupling strength on circulation patterns. The coupling strength is a monotonically decreasing function of the edge-to-edge distance d_e[15]. Thus for the hexagonal lattices, figure 3(a) shows a decreasing number of disks N_D forming a pattern region with increasing lattice spacing. The size depends strongly on the interaction strengths to overcome thermal agitations. The experiments performed at room temperature show a threshold edge-to-edge distance of

below 80 nm to order circulation states.
By using MTXM, we were able to get the average pattern size, however, their radial extent is missing. Therefore X-PEEM measurements were performed, which provided us a larger view on the lattice. The resulting XMCD pictures (not shown) are analyzed by calculating the spatial correlation $g(r)$, which is defined by[22]

$$g(r) =< c_i c_j > - < c_i >< c_j > . \quad (1)$$

Here, r denotes the distance between the disks i and j with vortex circulation $c_i(\pm 1)$ and $c_j(\pm 1)$. $< \cdots >$ represents a spatial average over all disk pairs separated by the same distance r, thus the correlation provides a non-local analysis. Figure 3(b) plots the correlation $g(r)$ as function of the distance for different edge-to-edge distances d_e calculated along the [10] axis. It gives us access to the length of the homocircular disk chains along [10] (upper axis in the plot). The vanishing correlation for large interdistances ($\mathrm{d}_e = 150$ nm) refers to the regime, where circulation patterns are destroyed due to thermal fluctuations. However for $\mathrm{d}_e = 100$ nm and particularly for $\mathrm{d}_e = 70$ nm the disks are positively coupled, corresponding to a homocircular configuration along [10], which is in agreement with the MTXM results. For measuring the correlation strength, a correlation length is defined as the distance, where $g(r)$ is decreased to $1/e$. Due to the expected alternating character of the correlation function along certain axes, the length was calculated for $|g(r)|$. The correlation length along different axes and the spatial average is plotted in figure 3(c) for the lattice with $\mathrm{d}_e = 70$ nm, initially saturated along [01]. Along all axes, the disks are coupled and most prominently along [10], which shows the homocircular chains. The spatial average as a measurement of the average radius of the circulation patterns is about 1 µm, corresponding to one disk in every direction, as expressed in the quantity N_R in the figure. To compare it with the MTXM results, N_R as a function of d_e is added in figure 3(a) assuming an isotropic pattern formation. The resulting average radius seems to be bigger, because the latter assumption is not accurate. The X-PEEM measurements show, that the patterns are formed but are not homogeneous along all axes (figure 3(c)). They are stretched along [10], resulting in a smaller average pattern radius.
In conclusion we have observed by X-ray imaging experiments, that circulation patterns are formed on a different energy scale than the scale of annihilation and nucleation field variations in vortex arrays. Micromagnetic simulations point to the reason, which is the interplay between the formation of flux-closure states during vortex nucleation and emerging circulation frustrations, where one favors order and the other disorder. The selection between the two regimes is controlled by the coupling strength and thermal fluctuations. It allows that the circulation state can still be degenerated (above d_e=100 nm), even though the annihilation and nucleation fields are strongly decreased by the vortex-vortex interaction. Our result can support the design of vortex data storage devices based on degenerated vortices and field sensor applications[4,23,24].

ACKNOWLEDGMENTS

This work was supported by the SFB668 of the German Science Foundation and the Cluster of Excellence 'The Hamburg Center for Ultrafast Imaging (CUI)'. The X-ray microscopy work at the ALS was funded by the U.S. Department of Energy, Office of Science, Basic Energy Sciences under Contract No. DE-AC02-05-CH11231. R.S., N.K. and P.F. acknowledge support from the U.S. Department of Energy, Office of Science, Basic Energy Sciences, Materials Sciences and Engineering Division under Contract No. DE-AC02-05-CH11231 (NEMM program MSMAG).

REFERENCES

[1] R. Wang, C. Nisoli, R. Freitas, J. Li, W. McConville, B. Cooley, M. Lund, N. Samarth, C. Leighton, V. Crespi, and P. Schiffer, Nature **439**, 303 (2006).
[2] V. Kruglyak and A. Kuchko, Physica B: Cond. Matt. **339**, 130 (2003).
[3] H. Puszkarski and M. Krawczyk, in *Interfacial Effects and Novel Properties of Nanomaterials*, Solid State Phenomena, Vol. 94 (Trans Tech Publications, 2003) pp. 125–134.
[4] B. Van Waeyenberge, A. Puzic, H. Stoll, K. W. Chou, T. Tyliszczak, R. Hertel, M. Fähnle, H. Brückl, K. Rott, G. Reiss, I. Neudecker, D. Weiss, C. H. Back, and G. Schütz, Nature **444**, 461 (2006).
[5] A. Fert, V. Cros, and J. Sampaio, Nature Nano. **8**, 152 (2013).
[6] R. Wiesendanger, Nature Rev. Mat. **1**, 16044 (2016).
[7] A. Soumyanarayanan, N. Reyren, A. Fert, and C. Panagopoulos, Nature **539**, 509 (2016).
[8] S. Jain, V. Novosad, F. Fradin, J. Pearson, V. Tiberkevich, A. Slavin, and S. Bader, Nature Comm. **3**, 1330 (2012).
[9] C. F. Adolff, M. Hänze, A. Vogel, M. Weigand, M. Martens, and G. Meier, Phys. Rev. B **88**, 224425 (2013).
[10] C. F. Adolff, M. Hänze, M. Pues, M. Weigand, and G. Meier, Phys. Rev. B **92**, 024426 (2015).
[11] C. Behncke, M. Hänze, C. F. Adolff, M. Weigand, and G. Meier, Phys. Rev. B **91**, 224417 (2015).
[12] S. Jain, Y. Ren, A. O. Adeyeye, and N. Singh, Phys. Rev. B **80**, 132401 (2009).
[13] R. Streubel, D. Makarov, F. Kronast, V. Kravchuk, M. Albrecht, and O. G. Schmidt, Phys. Rev. B **85**, 174429 (2012).
[14] R. Streubel, F. Kronast, C. F. Reiche, T. Mühl, A. U. B. Wolter, O. G. Schmidt, and D. Makarov, Appl. Phys. Lett. **108**, 042407 (2016).
[15] K. Y. Guslienko, V. Novosad, Y. Otani, H. Shima, and K. Fukamichi, Phys. Rev. B **65**, 024414 (2001).
[16] T. Miyata, Y. Minamino, S. Ida, and T. Minami, J. Vac. Sci. Technol. A **22**, 1711 (2004).
[17] R. Streubel, P. Fischer, F. Kronast, V. P. Kravchuk, D. D. Sheka, Y. Gaididei, O. G. Schmidt, and D. Makarov, J. Phys. D: Appl. Phys. **49**, 363001 (2016).
[18] T. Fischbacher, M. Franchin, G. Bordignon, and H. Fangohr, IEEE Trans. Mag. **43**, 2896 (2007).
[19] W. Hackbusch, *Hierarchische Matrizen: Algorithmen und Analysis* (Springer Science & Business Media, 2009).
[20] S. Börm, *Efficient numerical methods for non-local operators: H2-matrix compression, algorithms and analysis*, Vol. 14 (European Mathematical Society, 2010).

[21] R. Streubel, F. Kronast, U. K. Rößler, O. G. Schmidt, and D. Makarov, Phys. Rev. B **92**, 104431 (2015).
[22] W. Nolting, "Phasenübergänge," in *Grundkurs Theoretische Physik 6: Statistische Physik* (Springer Berlin Heidelberg, 2014) pp. 279–415.
[23] S. Bohlens, B. Krüger, A. Drews, M. Bolte, G. Meier, and D. Pfannkuche, Appl. Phys. Lett. **93**, 142508 (2008).
[24] J. Zimmer, A. Satz, W. Raberg, H. Brueckl, and D. Suess, "Device, magnetic sensor device and method," U.S. Patent 20150185297 A1 (2013).